Organic Electronics 122 (2023) 106889

Contents lists available at ScienceDirect

Organic Electronics

journal homepage: www.elsevier.com/locate/orgel

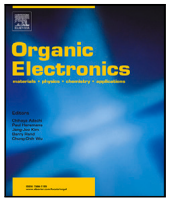

Method for instability compensation and detection of ammonium in sweat via conformal electrolyte-gated field-effect transistors

Mattia Petrelli [a,*], Bajramshahe Shkodra [a], Aniello Falco [a], Martina Aurora Costa Angeli [a], Sahira Vasquez [a], Alessandra Scarton [b], Silvia Pogliaghi [c], Roberto Biasi [b], Paolo Lugli [a], Luisa Petti [a]

[a] Sensing Technologies Laboratory (STL), Faculty of Engineering, Free University of Bozen-Bolzano, Bolzano, 39100, Italy
[b] Microgate Srl, Bolzano, 39100, Italy
[c] Department of Neuroscience, Biomedicine and Movement Science, University of Verona, Verona, 37100, Italy

ARTICLE INFO

Keywords:
Biosensors
Carbon nanotubes
Sweat sensing
Ion-selective membranes
Wearable electronics
Flexible electronics

ABSTRACT

The research interest towards wearable sensing devices has rapidly increased in recent years, due to the importance that personalized healthcare monitoring has gained in our everyday life. In this context, electrolyte-gated field-effect transistors (EG-FETs) for sensing applications are receiving increasing attention, owing to their intrinsic signal amplification and low operating voltages. Here, we report carbon nanotube EG-FETs (EG-CNTFET)-based sensors, functionalized with a nonactin-based ion-selective membrane for operation in an aqueous environment. In particular, we show a facile data analysis protocol to obtain a highly stable baseline response (i.e., 60 min) required for sensing applications. We successfully employ our EG-CNTFET-based sensors for the detection of ammonium (NH_4^+) in water, as well as in complex artificial sweat medium. Furthermore, we show how conditioning the membranes in artificial sweat significantly reduces the variability of the sensors. We achieve sensitivity as high as 1.797 μA/decade, with the linear range of the sensors entirely covering the physiological concentrations of NH_4^+ in sweat. We also show how increasing the nonactin concentration (from 0.2 to 1% wt) improves the sensors' sensitivity by a factor of 2.

1. Introduction

Over the past few years, wearable sensors have become more and more widespread, especially for the non-invasive, real-time monitoring of various physiological parameters, such as among others, heart rate, temperature, and blood pressure [1]. Thanks to the continuous effort towards miniaturization, wearable technology has emerged as a major component of the lifestyle- and fitness- markets, mostly in the form of smart bands and smartwatches, with accelerometer-based activity monitoring and photoplethysmography-based heart monitors among the most widely employed technologies [2].

Among the various sources of information of our physiological state, sweat is surely one of the most attractive ones. First, it is easily accessible from the skin without the need for invasive tools (e.g., needles). Secondly, being rich of metabolites, ions, proteins, and further biological indicators, it enables the extraction of a significant amount of information from its chemical composition [3,4]. For instance, glucose monitoring has been extensively explored, thanks to the excellent correlation between glucose levels in the blood and in the sweat [5–7]. Due to the growing interest towards noninvasive fatigue detection for sports applications, many groups have been working on the detection of biomarkers of interest for fatigue in the sweat. Historically, lactate has been regarded as possible biomarker for fatigue, and the possibility to monitor its concentration through sweat analysis has been extensively explored in the context of sport monitoring [8–10]. In the same framework, sodium (Na^+) and potassium (K^+) are among the most studied ions, since their concentrations are correlated to the hydration status [11,12]. In recent years, the concentration of ammonium (NH_4^+) in the sweat has been gaining increasing attention. It has been proposed, in fact, as an important parameter for biomedical applications [13], and its importance has been recently highlighted also in the context of sport monitoring.

Already in the early years of 1900s, the role of the accumulation of ammonia (NH_3) in the blood during physical exercise had been discussed [14,15]. The results from Czarnowski et al. validated the possibility of using the secretion of NH_3 in the sweat as an indicator of the starting point of the metabolic breakdown of the proteins, caused by the depletion of the carbohydrates [16–18]. In physiological conditions, the vast majority of NH_3 in the blood - ca. 98.3 % - is present

* Corresponding author.
E-mail address: mattia.petrelli@unibz.it (M. Petrelli).

https://doi.org/10.1016/j.orgel.2023.106889
Received 10 March 2023; Received in revised form 8 June 2023; Accepted 30 June 2023
Available online 3 July 2023

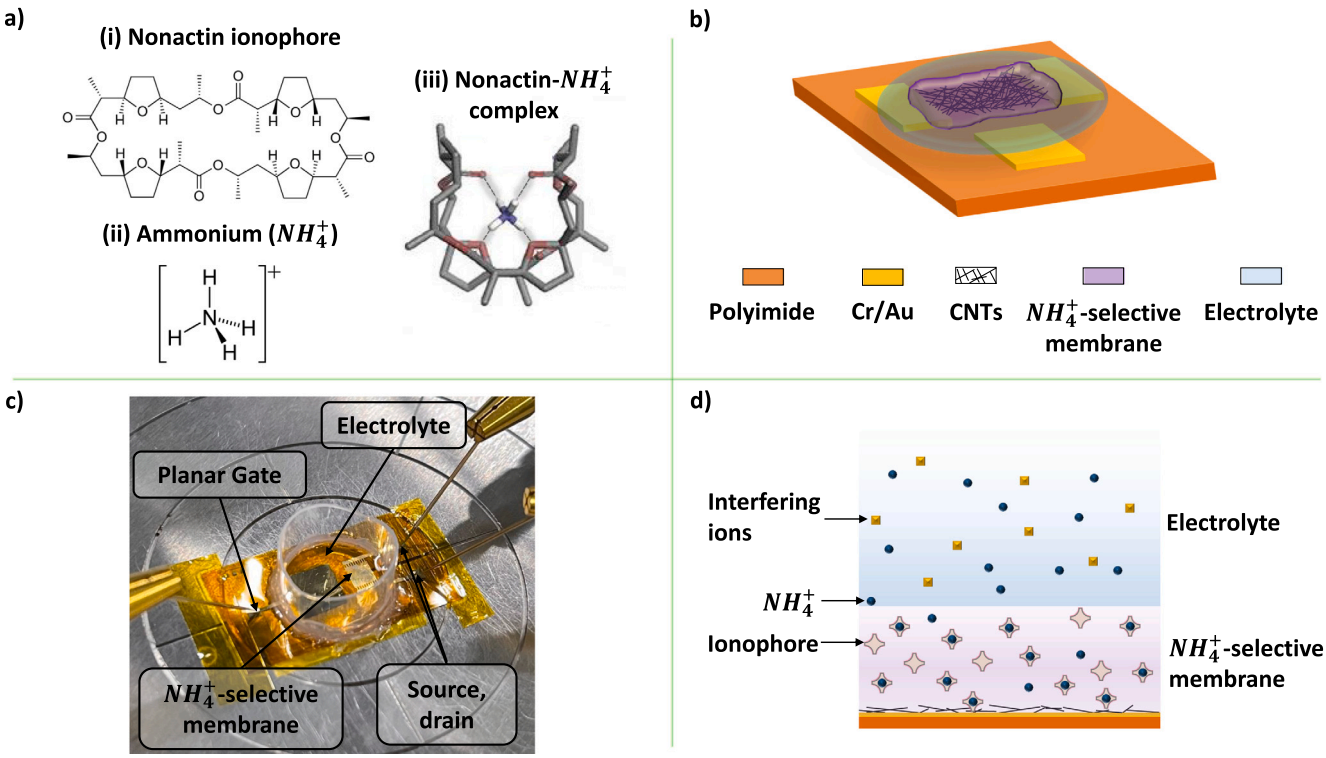

Fig. 1. (a) Chemical structure of (i) nonactin ionophore and (ii) ammonium (NH_4^+) cation. (iii) Nonactin-NH_4^+ complex, in which four hydrogen bonds are formed between the ionophore and the cation. (b) Schematic representation of the fabricated electrolyte-gated carbon nanotube field-effect transistor (EG-CNTFET)-based NH_4^+ sensors. (c) Picture of the fabricated EG-CNTFET-based NH_4^+ sensor placed on the probe station for electrical characterization. (d) Schematic cross-section of the working principle of the NH_4^+-selective membrane. The NH_4^+ cations present in the electrolyte are captured in the polymeric membrane in the binding sites created by the presence of the nonactin ionophore.

in the form of NH_4^+ [19]. The concentration of NH_4^+ can be hence used as a substitute to monitor the concentration of NH_3. More recent findings reported by other groups [20,21] have further confirmed the possibility of detecting, and hence possibly preventing, the onset of the catabolism of both blood and muscle organic proteins by monitoring the concentration of NH_4^+ in the sweat.

In general, the detection of ions is carried out by means of ion-selective membranes, which are based on polymeric materials. Membranes achieve sensitivity and selectivity thanks to the presence of ionophores. In the specific case of the detection of NH_4^+, nonactin is the most employed ionophore for the preparation of potentiometric electrochemical sensors. Other ionophores have been tested through the years, as well as ionophore-free approaches, but they do not guarantee the same sensing performance of nonactin [13]. The working mechanism of the interaction between the nonactin and NH_4^+ is schematically depicted in Fig. 1a: when NH_4^+ is in proximity of the nonactin, there is the formation of four hydrogen bonds between the four hydrogen atoms of NH_4^+ and four oxygen atoms of the nonactin. This results in a structural rearrangement of the nonactin around the NH_4^+ cation and the formation of a stable nonactin-NH_4^+ complex, leading to sensitive and selective NH_4^+ sensing [13,22].

The most widespread methodology for the sensing of NH_4^+ in the sweat is based on electrochemical sensors, functionalized with NH_4^+-selective membranes [23–25]. Nonetheless, different approaches have been recently explored for the development of NH_4^+ sensors, e.g., sensors based on organic electrochemical transistors [26] or conductive threads [27]. One of the most promising transducing platform for biosensing applications and, specifically, for sweat analysis is represented by electrolyte-gated field-effect transistors (EG-FETs) [28]. The working principle of EG-FETs, which relies on the formation of two electrical double layers at the semiconducting channel-electrolyte and the gate contact-electrolyte interfaces, allows device functionality $< |1|$ V, crucial for sweat sensing, considering that the electrolysis of water occurs at 1.23 V at 25 °C and 1 atm [29–31]. Moreover, the intrinsic large gate capacitance entails a great signal amplification, which allows sensitive detection of small molecules [32,33]. Different materials have been tested as active layers for EG-FETs [34]. Among them, carbon nanotubes (CNTs) exhibit manifold attractive properties (high surface-to-volume ratio, possibility of functionalization with different types of bio-recognition elements, possibility of deposition on a wide range of substrates using low-cost techniques such as printing) [35]. Carbon nanotube EG-FETs (EG-CNTFETs) have been therefore extensively used for the fabrication of highly sensitive platforms for the detection of analytes in liquid phase [36–38].

In general, stability is one of the main challenges to be tackled in the design of a EG-FET-based sensing platform [28]. One of the most common approaches reported in literature for EG-CNTFETs is the use of polymer-based coatings, that insulate as much as possible the device from the electrolyte. Being the CNTs no longer in direct contact with the electrolyte, the modulation of their conductivity by the ions in solution is significantly reduced, hence providing stable electrical characteristics [39,40].

In this respect, the ion-selective membrane employed for the functionalization of the EG-CNTFETs allowed not only achieving the desired selectivity and sensitivity, but also in providing encapsulation. To methodologically address the stability issue, and allow a reliable detection of the biosensing data, we designed a facile data analysis protocol. The drift deriving from the instability was successfully subtracted from the response of the devices and it was therefore possible to correctly extract the calibration curve of the proposed EG-CNTFET-based sensors.

Herein, a thorough analysis of the fabrication and characterization of EG-CNTFET-based NH_4^+ sensors is reported. A schematic representation of the devices is depicted in Fig. 1b: semiconducting CNTs were employed as active layer, and a nonactin-based ion-selective membrane was used for the functionalization of the devices, to ensure sensitive and selective NH_4^+ detection. The article is structured as follows. First,

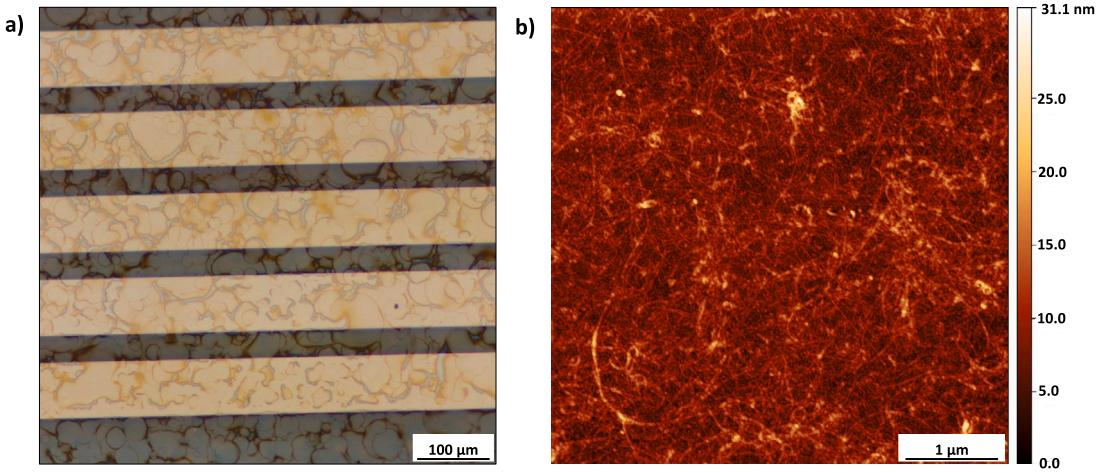

Fig. 2. (a) Optical microscope of the as spray-deposited carbon nanotubes-carboxymethyl cellulose (CNTs-CMC) dispersion on the interdigitated source and drain electrodes on the flexible polyimide (PI) substrate. The diameter and distribution of the droplets are indicative of the goodness of the deposition and, hence, of the uniformity of the resulting CNT random network. (b) Atomic force microscope (AFM) micrograph of the spray-deposited CNTs, after the removal of the CMC matrix through the $HNO_3 + H_2O$ *treatment*. It can be observed how there is no formation of CNT bundles during the deposition process and/or after the removal of the surfactant.

multiple fabrication and characterization procedures (e.g., different conditioning solutions, different membrane composition) are introduced. Subsequently, the results of the characterization of different devices by means of physical, chemical, and electrical tests are presented. The influence of the presence of the NH_4^+-selective membrane was investigated. The stability of the devices was carefully assessed, and a reliable data processing protocol was proposed. Finally, the devices were tested for the detection of NH_4^+ over the concentration range from 0.01 mM to 100 mM, to entirely cover the range of concentrations observed during physical activity [21]. For the optimal combination of fabrication parameters, average sensitivity of 1.797 µA/decade was achieved, with a reduction of the relative standard deviation greater than 50 %, and a coefficient of determination of 88.03 %.

2. Materials and methods

All chemicals were purchased from Sigma-Aldrich, unless otherwise stated. All solutions and dispersions were prepared using deionized H_2O with a resistivity of 18.2 MΩ*cm produced by a Milli-Q system (Millipore, SAS, France).

2.1. EG-CNTFETs fabrication

The EG-FET layout consists of interdigitated source and drain gold electrodes (IDEs) as source and drain (L = 50 µm, W = 57 mm) and a planar gold gate electrode [41]. The CNTs were prepared for the spray deposition process in the form of a water-based solution, in which 0.05 %wt CNTs (95 % semiconducting, median length 1 µm, average diameter 0.78 nm, Merck KGaA, Darmstadt, Germany) were dispersed using 0.5 %wt sodium carboxymethyl cellulose (CMC) as surfactant [42,43]. The detailed description on the fabrication of the EG-CNTFET and the spray deposition of the semiconducting CNTs are given in Section 1.1 of the Supporting Information, while a schematic representation is reported in Figure S1.

The quality of the spray-deposited CNT layers was checked by optical microscope (Axio Imager, Carl Zeiss Microscopy GmbH, Germany) immediately after the spray deposition process and atomic force microscope (AFM) imaging (Nanosurf CoreAFM, Switzerland) after the removal of the CMC.

2.2. EG-CNTFETs functionalization

To achieve selective detection of NH_4^+, the fabricated EG-CNTFET devices were functionalized by drop-casting of a nonactin-based NH_4^+-selective membrane. The membrane was prepared following the protocol reported in [23], with modifications. The details on membrane preparation and subsequently device functionalization are given in section 1.2 of the Supporting Information.

2.3. EG-CNTFET-based sensors characterization

The electrical characterization was performed by means of a probe station, connected to a Keysight B1500A Semiconductor Device Parameter Analyzer. All the tests were run at room temperature and in ambient air conditions, using deionized H_2O or artificial sweat, depending on the specific test, applying the characterization procedures introduced in our previous works [44,45]. All the details regarding the biasing voltages applied and the characterization protocols can be found in section 1.3 of the Supporting Information.

3. Results and discussion

3.1. Morphological characterization

An optical microscope picture of the CNT solution, immediately after the spray deposition on the IDE of the devices, is reported in Fig. 2a. It can be observed how the achieved deposition regime is the intermediate one, in which the droplets of the atomized solution arrive at the substrate and, thanks to the beneficial effect of the plasma treatment of the surface before the spray deposition [42], can spread and merge to form a smooth and uniform layer. The goodness of the deposition was further corroborated by means of AFM imaging after the $HNO_3 + H_2O$ *treatment*: as shown in Fig. 2b, the CNT network is bundle-free, dense and uniform across the surface. Furthermore, the distribution is and the surfactant matrix is completely removed by the $HNO_3 + H_2O$ *treatment*.

3.2. Impact of the NH_4^+-selective membrane on the electrical characteristics of the EG-CNTFETs

Prior to the characterization of the fabricated sensors towards the detection of the NH_4^+, we investigated the effect of the presence of the ion-selective membrane on the electrical properties of the CNTs

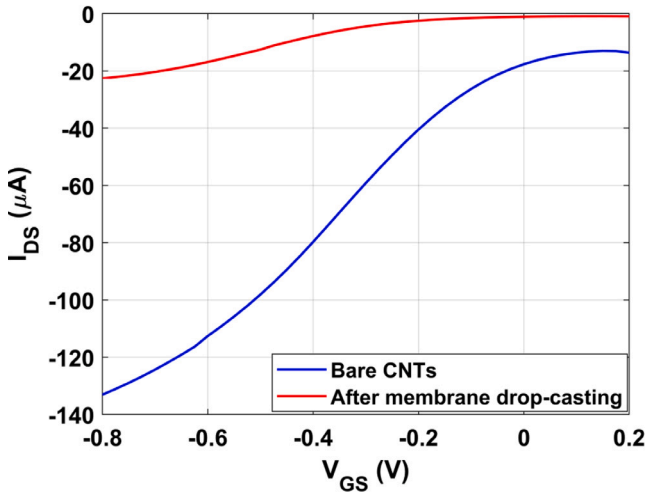

Fig. 3. Transfer characteristics of the EG-CNTFET before and after the drop-casting of the NH_4^+-selective membrane, measured while keeping the drain–source voltage V_{DS} fixed at −0.1 V and with 200 μL of deionized water as electrolyte.

that form the semiconducting channel. For all the fabricated devices, the drain–source resistance R_{DS} increased minimum 15-fold after the drop-casting of the NH_4^+-selective membrane, with respect to the initial value measured immediately after the *$HNO_3 + H_2O$ treatment*. This is to be ascribed to the penetration of the polymeric membrane, inherently insulating, into the CNT network, with the consequent reduction of the number of conductive paths and the overall reduction of the network conductivity.

To further investigate the impact of the presence of the membrane on the performance of the devices, we fabricated a separate batch of N = 4 devices, to characterize them in terms of I_{ON}/I_{OFF} ratio and sub-threshold swing SS, by recording the transfer characteristics before and after the drop-casting of the NH_4^+-selective membrane. It is important to mention that, for this specific test, the conditioning step was not performed, for the purpose of investigating only the effect of the drop-casting of the membrane on the electrical performance of the CNTs. The transfer characteristics for one of these devices, recorded before and after the drop-casting of the membrane and representative of the behavior of all of them, is presented in Fig. 3, while the complete electrical characteristics are summarized in figure S2. The average value of R_{DS} increased from 1.08 kΩ (relative standard deviation of 5.5 %) before the application of the membrane to 15 kΩ (relative standard deviation of 32.19 %), with a ca. 14-fold increase. The I_{ON}/I_{OFF} ratio improved from an average of 9.38 A/A to an average of 21.94 A/A (relative standard deviation of 66.40 % and 32.41 %, respectively), while the SS improved from an average of 831 mV/decade to an average of 600 mV/decade (relative standard deviation of 16.54 % and 17.68 %, respectively). This improvement in the overall electrical performance of the EG-CNTFETs, at the cost of a reduction of the channel conductivity and, hence, of the I_{ON} of the devices, is compatible with what was reported by Joshi et al. in [40]. From these results, we could conclude that to have reliable EG-CNTFET operation (i.e., the I_{ON} at least two orders of magnitude above the gate current I_G) after the drop-casting of the NH_4^+-selective membrane, it is fundamental to optimize the parameters of the spray deposition to obtain a semiconducting channel with R_{DS} <10 kΩ, in accordance with our previous findings reported in [46], obtained for a different functionalization strategy.

3.3. Stability of the EG-CNTFET-based NH_4^+ sensors

One of the most critical aspects of EG-CNTFET-based sensors is the stability during the measurement. The presence of the electrolyte, in fact, while being necessary for the operation of the devices, is at the same time source of instability and drift in the drain–source current I_{DS} [28,39]. For this reason, we have characterized our EG-CNTFET-based sensors (i.e., the EG-CNTFETs functionalized with the NH_4^+-selective membrane) in real-time, to understand if, and when, the response of the devices would reach a stable behavior.

The typical trend of I_{DS} and I_G for all the sensors tested using H_2O as electrolyte is depicted in Fig. 4a. At the start of the measurement, the two currents undergo very quick changes, because of the initial major re-arrangement of the ions and the formation of the two electrical double layers at the semiconducting channel-electrolyte and the gate contact-electrolyte interfaces. After this initial phase, the I_{DS} quickly recovers to the initial value and then starts increasing in absolute value. We defined the first 60 min of the measurement as *stabilization phase*. After 1 h of continuous measurement, there is the onset of what we defined as the *constant slope phase*, i.e., the onset of a stable linear trend in the increase of the I_{DS} in absolute value. The two phases of the measurement are highlighted in 4b. This is similar to what was reported by Molazemhosseini et al. for similar classes of CNT-based biosensors, in which deionized H_2O was used as gating medium [39]. Since the increase in the absolute value of I_{DS} over time is not negligible, it was hence necessary to subtract it to correctly obtain the response of the device to the additions of NH_4^+. The linear fitting of this baseline was obtained by taking the I_{DS} in the *constant slope phase*, i.e., between 60 and 100 min (for all the devices tested, the average R^2 was 96.29 %, with a relative standard deviation of 6.30 %). By subtracting this stable baseline from the overall trend of the I_{DS}, the corrected response I^*_{DS}, shown in Fig. 4c, was obtained.

During the *stabilization phase* of the I_{DS}, the gate current I_G goes through a similar stabilization, most probably due to the continuous re-arrangement of the ions in the electrolyte in response to the applied gate–source voltage V_{GS}. Most importantly, as visible in Fig. 4d, I_G lies in the <10 nA range (in absolute value) during the whole measurement time, proving low leakage and reliable EG-CNTFET operation of the tested devices [36].

3.4. Characterization towards NH_4^+ in H_2O: effect of conditioning

In Fig. 5, the average calibration curve extracted for the devices conditioned and characterized using deionized H_2O as electrolyte is reported (red circle markers). The corrected response I^*_{DS} of the tested devices is linear from 0.01 mM to 10 mM: in this range of concentrations, it shows an average sensitivity of 0.1 μA/decade and a coefficient of determination of 96.96 %. It can be clearly seen how the response diverges from linearity when the last concentration (100 mM) was tested, showing signs of saturation, and for this reason this last concentration was excluded from the calculation of the reported data. Nevertheless, the physiological range of concentrations of NH_4^+ in sweat (0.12 – 2.17 mM [21]) is completely covered by the linear range of the tested sensors.

The increase shown by the corrected response I^*_{DS} can be explained by referring to the working principle of the EG-CNTFET platform and of the ion-selective membrane. In normal conditions, the semiconducting channel is rich of positive charge carriers thanks to the p-type behavior of the semiconducting CNTs. When NH_4^+ ions are present in the electrolyte, they are captured by the ionophore and trapped inside the ion-selective membrane (Fig. 1d). By diffusing inside the membrane, the NH_4^+ cations arrive at a distance below the Debye length λ_D from the semiconducting channel. The accumulation of enough of these NH_4^+ cations, in turn, leads to the depletion of positive charge carriers from the semiconducting CNT channel. This can be regarded as a shift in the threshold voltage of the device and, by consequence, a reduction in the overall device conductivity [36].

As already described in Section 2.3, the additions of the different concentrations of NH_4^+ were performed with intervals of 10 min. It is important to point out how the extraction of the calibration curve was carried out by averaging over the last 5 min of each interval. The first

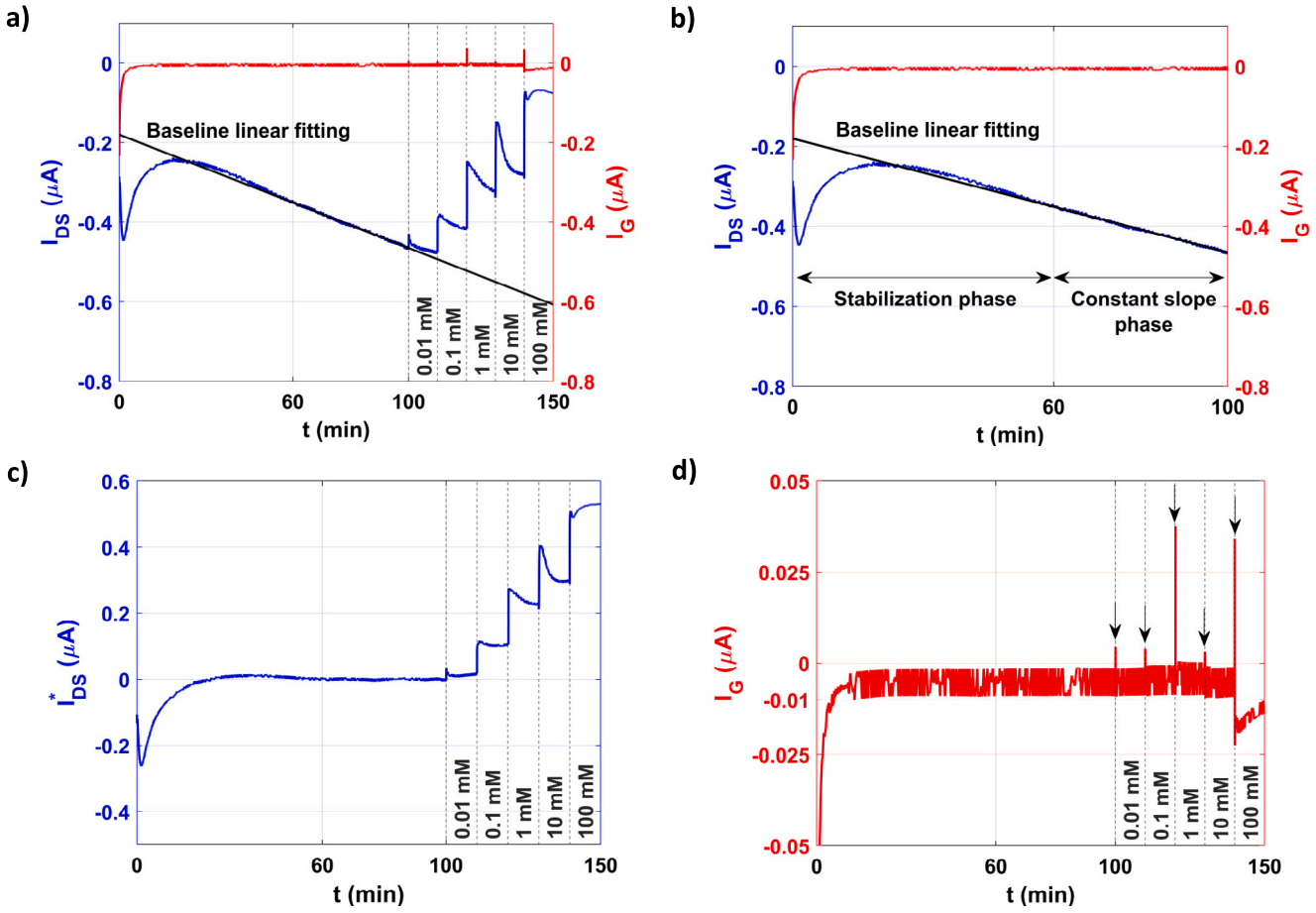

Fig. 4. (a) Representative real-time measurement of the drain–source current I_{DS} (blue line) and of the gate current I_G (red line), for fixed V_{GS} = −0.8 V and V_{DS} = −0.1 V, for all the devices tested using H_2O as electrolyte. The black line represents the linear fitting of the I_{DS} calculated after 60 min of continuous measurement (R^2 >99 %, for this specific device). The additions of the increasing NH_4^+ concentrations (reported in the plot) are in correspondence with the dashed lines (t = 100; 110; 120; 130; 140 min). (b) Zoom-in of the real-time measurement shown in panel (a), with highlighted the *stabilization phase* and the *constant slope phase*. The linear fitting (black line) of the baseline is calculated by considering the I_{DS} in the *constant slope phase*. (c) Corrected drain–source current I^*_{DS} (i.e., I_{DS} after the baseline subtraction), used for the extraction of the calibration curve. (d) Zoom-in of the real-time measurement for the gate current I_G. The spikes (pointed by the arrows) correspond to the instants of the NH_4^+ additions.

5 min were discarded to exclude the effect of the spikes in the I_{DS} that occur immediately after each addition of a new concentration of NH_4^+ (clearly visible in Fig. 4c). These spikes can be observed also in the gate current, as shown in Fig. 4d. At the moment of the addition of each new concentration, in fact, there is an instantaneous perturbation of the electrical double layers, both because of the combined effects of the mechanical action of the drop-casting and the introduction of new ions in the electrolyte. Therefore, in the immediate aftermath of the drop-casting, the ions in the bulk of the electrolyte are dragged by the applied V_{GS}, effectively causing a spike in the gate current I_G. While for the I_G the amplitude of this spike is still in the nA range, so it is very quick to recover, the same does not hold for the I_{DS}, where several minutes are required for the transient phase to be completely extinguished.

As well reported in literature, the conditioning step is important to guarantee a stable response of membrane-based potentiometric sensors [23], due to the intake of H_2O, primary ions, and interfering ions [47]. Nevertheless, it is a long process step (it can require up to several hours for poly(vinyl chloride)-based membranes). We tried then to investigate if for our configuration it was possible to skip the conditioning step. Fig. 5 reports the direct comparison of two batches of devices, one fabricated by employing the conditioning in 1 mM NH_4^+ in deionized H_2O and the other fabricated by skipping entirely the conditioning. The average sensitivity of the devices conditioned in 1 mM NH_4^+ was more than 3-fold with respect to one of the devices for which the conditioning step was not performed (0.1 μA/decade vs 0.033 μA/decade, respectively). Moreover, while the linear range of the response was the same for both experiments, the devices that were not conditioned showed a much higher relative standard deviation for the average sensitivity (35.78 % with respect to 2 %) and a lower coefficient of determination (88.30 % with respect to 96.96 %). Therefore, the conditioning step was kept as part of the fabrication protocol.

3.5. Selectivity analysis: characterization in artificial sweat

To explore the selectivity of the fabricated EG-CNTFET-based sensors and test them in conditions closer to the real-life settings for a wearable device, we repeated the characterization towards NH_4^+ employing artificial sweat as electrolyte. All the considerations reported in Section 3.3 regarding the *stabilization phase* and the *constant slope phase*, as well as the extraction of the sensor response after the subtraction of the baseline linear fitting, remained valid. The devices, in fact, showed the same behavior during the tests (representative measurements in artificial sweat are reported in Figure S3). This is a further proof of the robustness of the proposed approach for the data extraction, also in the case of the devices characterized using artificial sweat as electrolyte.

In Fig. 6, the average calibration curve extracted for the devices characterized using artificial sweat as electrolyte is reported (magenta diamond markers). The corrected response I^*_{DS} was linear from 0.1 mM to 100 mM, with an average sensitivity of 1.358 μA/decade and a coefficient of determination of 85.57 %. Compared to the devices tested using H_2O as electrolyte (Fig. 5), the lowest concentration tested (0.01 mM)

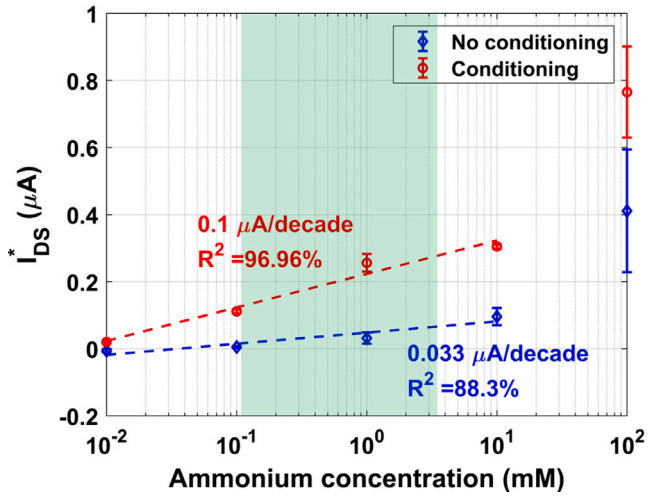

Fig. 5. Calibration curves representing the average corrected response of the EG-CNTFET-based sensors (I^*_{DS}) vs different concentrations of NH_4^+, to investigate the effect of the conditioning of the NH_4^+-selective membrane. All the devices were tested using deionized H_2O as electrolyte. The green box highlights the physiological range of concentrations of NH_4^+ during physical exercise [21]. The response of the devices towards NH_4^+ diverged from linearity when the highest concentration (100 mM) was tested, showing signs of saturation. The average sensitivity of the devices conditioned in 1 mM NH_4^+ (red circle markers) is more than 3-fold with respect to the average sensitivity of the devices without conditioning (blue diamond markers). Here, the error bars represent the standard errors of the mean, with N = 2 devices without conditioning and N = 3 devices with conditioning.

was not anymore covered by the linear range of the devices. On the other hand, there was no sign of saturation for the highest concentration tested (100 mM). This loss of sensitivity at the lowest concentration is to be ascribed to the different Debye length λ_D in artificial sweat, compared to the one in deionized H_2O. In fact, the calculated λ_D for the deionized H_2O was 50 nm (mainly attributed to the formation of carbonic acid), while for the prepared artificial sweat, because of the large presence of the ionic species, we calculated a λ_D of 1.57 nm (the complete calculations can be found in the Supporting Information). It is important to remember that the Debye length λ_D is the distance after which the charges in the electrolyte are completely screened [48], and it represents one of the major limitations for EG-FET-based sensors: only the molecules present at a distance lower than λ_D from the semiconducting channel contribute to the modulation of the I_{DS}. Hence, working in high ionic environments, where the λ_D is in the low-nm range (like in the case of artificial sweat), is extremely challenging. It represents therefore a major achievement the fact that the proposed devices, despite the shift towards higher concentrations of the linear range, are able to detect the physiological range of concentrations of NH_4^+ in sweat, proving the feasibility of the proposed approach.

In an attempt to improve the performance of the devices, we employed a different conditioning procedure: instead of using a 1 mM NH_4^+ solution in deionized H_2O, we performed the conditioning step in a 1 mM NH_4^+ solution in artificial sweat. In this way, the membrane would be exposed not only to the target ions, but also to the interfering species during the conditioning [47,49]. To the best of our knowledge, this was the first time this approach was applied for the fabrication of EG-CNTFET-based sensors. As reported in Fig. 6a, the response of the devices fabricated using this different conditioning medium (black circle markers) showed linearity in the same range of NH_4^+ concentrations (from 0.1 mM to 100 mM), with an improved average sensitivity of 1.797 μA/decade and coefficient of determination of 88.03 %. Most importantly, the relative standard deviation for the average sensitivity of these devices was significantly lower compared to the one of the devices for which the conditioning was carried out in deionized H_2O: 59 % with respect to 139 %. Conditioning the NH_4^+-selective membrane in the same electrolyte to which it will be exposed during the real testing leads to less variability in the performance of the EG-CNTFET-based sensors. This is in agreement with what reported in [49] for Pb^{2+}- and Ca^{2+}-selective membranes and in [47] for K^+- and Ca^{2+}-selective membranes: the incorporation in the membrane of interfering ions, together with target ions, leads to better sensing characteristics of the ion-selective membrane, compared to the case in which the conditioning is performed only with target ions.

While linearity is a desirable characteristic for a biosensor, several studies have been reported in which a quadratic fitting of the experimental data provides a better R^2 [50], [51]. A similar approach was thus employed for further analysis of the data presented in this section, and the results are summarized in Figure 6b. The coefficient of determination was R^2 >99.9 % both for the devices conditioned in H_2O and the devices conditioned in artificial sweat. The sensitivity can be extracted as:

$$S(x) = \frac{\partial y}{\partial x} \tag{1}$$

obtaining

$$S(x) = -0.0012x + 0.1567 \tag{2}$$

for the devices conditioned in H_2O, and

$$S(x) = -0.0017x + 0.2184 \tag{3}$$

for the devices conditioned in artificial sweat. Given that the devices were tested with the same range of concentrations of NH_4^+ (i.e., the values of x), it is straightforward to conclude that conditioning in artificial sweat leads to higher sensitivity. The quadratic fitting covered all the range of concentrations tested. This would allow for precise prediction of the concentration present in the electrolyte, e.g., by means of post-processing algorithms or of a look-up table.

3.6. Change in membrane composition

In an attempt to expand the linear range of the fabricated EG-CNTFET-based NH_4^+ sensors towards lower concentrations and further improve the sensitivity, we modified the composition of the NH_4^+-selective membrane mixture. Being the ionophore the element responsible for the sensitivity and selectivity of the membrane, we increased its concentration in the membrane mixture, from the previous 0.2 %wt to 1 %wt. We fabricated a new batch of N = 5 devices, for which we employed the conditioning step in artificial sweat, in light of the findings reported in Section 3.5. The average calibration curve for this batch of devices is depicted in Figure S4. The response was linear in the same range as the other devices conditioned in artificial sweat (from 0.1 mM to 100 mM), with an improved average sensitivity of 3.585 μA/decade (a 99.5 % increase with respect to the devices fabricated with the membrane containing 0.2 %wt of ionophore) and coefficient of determination of 87.66 %, and a higher relative standard deviation for the sensitivity (66 %). As expected, increasing the concentration of the ionophore led to higher sensitivity, but only ~2-fold, compared to the 5-fold increase in the concentration of the ionophore. Assuming that the concentration of the ionophore is proportional to the number of sites available in the membrane for the capture of the NH_4^+ ions, it is fair to assume that a saturation of the possible available number of sites occurred: increasing above a certain threshold the concentration of the ionophore does not lead to significant improvement in the sensitivity of the sensors. Considering that the ionophore is by far the most expensive element of the membrane mixture, an optimization of its concentration in the preparation of the membrane mixture would be required to maximize the sensitivity of the devices without exceeding the maximum quantity of ionophore necessary.

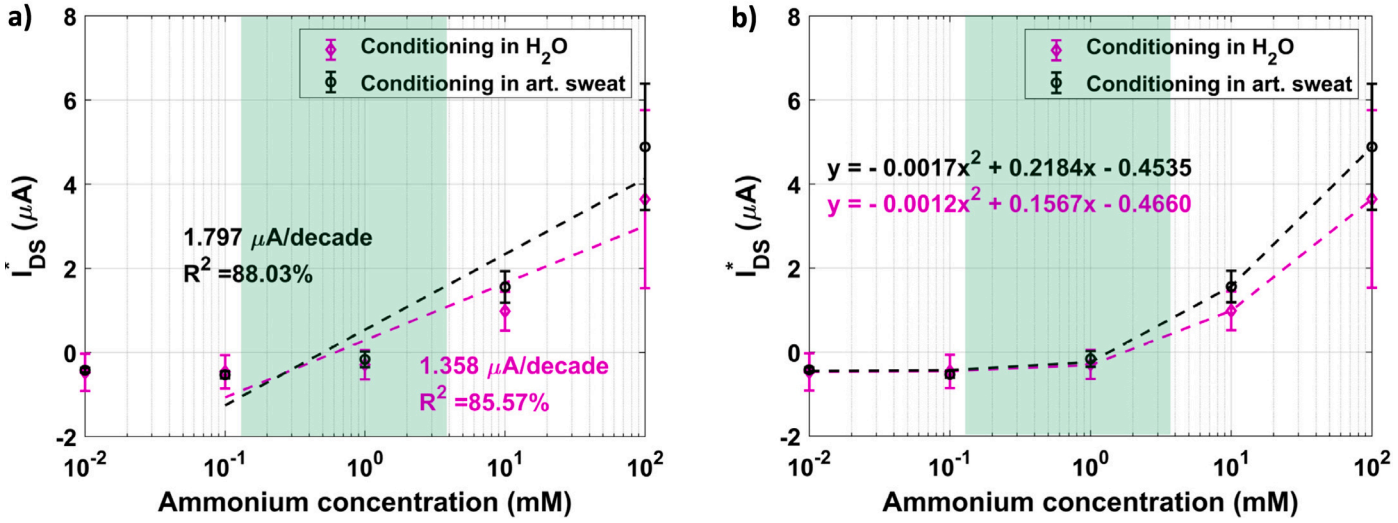

Fig. 6. Calibration curves representing the average corrected response of the EG-CNTFET-based sensors (I^*_{DS}) vs different concentrations of NH_4^+, to investigate the effect of different conditioning solutions of the NH_4^+-selective membrane, analyzed by means of (a) linear fitting and (b) quadratic fitting. All the devices were tested using artificial sweat as electrolyte. The green box highlights the physiological range of concentrations of NH_4^+ during physical exercise [21]. The average sensitivity of the devices conditioned in 1 mM NH_4^+ in artificial sweat (black circle markers) is higher compared to the one of the devices conditioned in 1 mM NH_4^+ in deionized H_2O (magenta diamond markers). Here, the error bars represent the standard errors of the mean, with N = 5 devices for both batches.

4. Conclusions

In this work, we report a complete analysis of flexible, planar EG-CNTFET-based NH_4^+ sensors for sweat analysis. We studied the effect of the presence of the membrane on the electrical properties of the device, as well as a facile, reliable protocol to eliminate the drift of the drain–source current I_{DS} from the analysis of the sensing characteristics of the devices. The importance of the conditioning step for the sensing properties of the NH_4^+-selective membrane performance was studied: the devices for which the conditioning was performed showed higher sensitivity and improved linearity, even more so when the conditioning was performed in artificial sweat. Furthermore, the devices were tested also in highly complex environment such as artificial sweat, to mimic the real-life working conditions for which these sensors are designed.

Table 1 summarizes the main results obtained for all the devices tested in artificial sweat. For all of them, the linear range completely covered the physiological range of concentrations of interest for NH_4^+ in the sweat. As discussed in the Results section, performing the conditioning step in artificial sweat led to better performance of the sensors, increasing their sensitivities and reducing to less than half their relative standard deviation. Increasing the concentration of the ionophore in the membrane mixture improved the sensitivity as well, but not enough to justify the extra cost derived from the higher quantity of material used.

The results reported in this work constitute a solid basis for the development of highly sensitive and selective NH_4^+ sensors for sweat analysis. Future work will be focused on the design of a custom readout circuitry [52] and of a dedicated microfluidics system, to achieve a complete portable system for the testing of EG-CNTFET-based sensors in real-time on human subjects.

Table 1
EG-CNTFET-based NH_4^+ sensors parameters, comparing different conditioning procedures and NH_4^+-selective membranes compositions. For all the considered devices, the linear range was from 0.1 mM to 100 mM, covering entirely the physiological range of concentrations of NH_4^+ in sweat.

Conditioning medium	Ionophore %wt	Avg. Sensitivity [μA/decade]	Sensitivity re-STD [%]	R^2 [%]
H_2O	0.2	1.385	139	85.57
Art. sweat	0.2	1.797	59	88.03
Art. sweat	1	3.585	66	87.66

CRediT authorship contribution statement

Mattia Petrelli: Conceptualization, Methodology, Software, Validation, Formal analysis, Investigation, Data curation, Visualization, Writing – original draft. **Bajramshahe Shkodra:** Conceptualization, Methodology, Investigation, Visualization, Writing – original draft. **Aniello Falco:** Conceptualization, Methodology, Validation, Writing – review & editing. **Martina Aurora Costa Angeli:** Conceptualization, Supervision, writing – review & editing. **Sahira Vasquez:** Methodology, Validation, Writing – review & editing. **Alessandra Scarton:** Writing – review & editing. **Silvia Pogliaghi:** Writing – review & editing. **Roberto Biasi:** Funding acquisition, Writing – review & editing. **Paolo Lugli:** Funding acquisition, Project administration, Writing – review & editing. **Luisa Petti:** Supervision, Project administration, Writing – review & editing.

Declaration of competing interest

The authors declare that they have no known competing financial interests or personal relationships that could have appeared to influence the work reported in this paper.

Data availability

Data will be made available on request

Acknowledgments

The authors would like to thank Prof. Sandro Carrara and Dr. Ata Golparvar of the Bio/CMOS Interfaces Group, École Polytechnique Fédérale de Lausanne (EPFL), Switzerland, for the input and the great discussions about biosensors and sweat analysis.

This work was partially funded by the Autonomous Province of Bolzano-South Tyrol's European Regional Development Fund (ERDF) Program (project codes EFRE/FESR 1068-Senslab and EFRE/FESR 1127-STEX), the EYRe project of the Faculty for Science and Technology of Free University of Bozen-Bolzano, and Istituto Italiano di Tecnologia (IIT).

Appendix A. Supplementary data

Supplementary material related to this article can be found online at https://doi.org/10.1016/j.orgel.2023.106889.

References

[1] I. Cheol Jeong, D. Bychkov, P.C. Searson, Wearable devices for precision medicine and health state monitoring, IEEE Trans. Biomed. Eng. 66 (5) (2018) 1242–1258.

[2] E. Mencarini, A. Rapp, L. Tirabeni, M. Zancanaro, Designing wearable systems for sports: A review of trends and opportunities in human–computer interaction, IEEE Trans. Hum.–Mach. Syst. 49 (4) (2019) 314–325.

[3] A.J. Bandodkar, W.J. Jeang, R. Ghaffari, J.A. Rogers, Wearable sensors for biochemical sweat analysis, Annu. Rev. Anal. Chem. 12 (2019) 1–22.

[4] R. Ghaffari, J.A. Rogers, T.R. Ray, Recent progress, challenges, and opportunities for wearable biochemical sensors for sweat analysis, Sensors Actuators B 332 (2021) 129447.

[5] J. Moyer, D. Wilson, I. Finkelshtein, B. Wong, R. Potts, Correlation between sweat glucose and blood glucose in subjects with diabetes, Diabetes Technol. Therapeutics 14 (5) (2012) 398–402.

[6] H. Lee, C. Song, Y.S. Hong, M. Kim, H.R. Cho, T. Kang, K. Shin, S.H. Choi, T. Hyeon, D.-H. Kim, Wearable/disposable sweat-based glucose monitoring device with multistage transdermal drug delivery module, Sci. Adv. 3 (3) (2017) e1601314.

[7] S.M. Khor, J. Choi, P. Won, S.H. Ko, Challenges and strategies in developing an enzymatic wearable sweat glucose biosensor as a practical point-of-care monitoring tool for type II diabetes, Nanomaterials 12 (2) (2022) 221.

[8] T. Saha, T. Songkakul, C.T. Knisely, M.A. Yokus, M.A. Daniele, M.D. Dickey, A. Bozkurt, O.D. Velev, Wireless wearable electrochemical sensing platform with zero-power osmotic sweat extraction for continuous lactate monitoring, ACS Sensors 7 (7) (2022) 2037–2048.

[9] E. Yüzer, V. Doğan, V. Kılıç, M. Şen, Smartphone embedded deep learning approach for highly accurate and automated colorimetric lactate analysis in sweat, Sensors Actuators B 371 (2022) 132489.

[10] S. Tonello, T. Fapanni, S. Bonaldo, G. Giorgi, C. Narduzzi, A. Paccagnella, M. Serpelloni, E. Sardini, S. Carrara, Amperometric measurements by a novel aerosol jet printed flexible sensor for wearable applications, IEEE Trans. Instrum. Measur. (2022).

[11] M. Parrilla, R. Cánovas, I. Jeerapan, F.J. Andrade, J. Wang, A textile-based stretchable multi-ion potentiometric sensor, Adv. Healthc. Mater. 5 (9) (2016) 996–1001.

[12] F. Criscuolo, I.N. Hanitra, S. Aiassa, I. Taurino, N. Oliva, S. Carrara, G. De Micheli, Wearable multifunctional sweat-sensing system for efficient healthcare monitoring, Sensors Actuators B 328 (2021) 129017.

[13] M. Cuartero, N. Colozza, B.M. Fernández-Pérez, G.A. Crespo, Why ammonium detection is particularly challenging but insightful with ionophore-based potentiometric sensors–An overview of the progress in the last 20 years, Analyst 145 (9) (2020) 3188–3210.

[14] B. Mutch, E. Banister, Ammonia metabolism in exercise and fatigue: A review, Med. Sci. Sports Exerc. 15 (1) (1983) 41–50.

[15] D.J. Wilkinson, N.J. Smeeton, P.W. Watt, Ammonia metabolism, the brain and fatigue; Revisiting the link, Progress in Neurobiology 91 (3) (2010) 200–219.

[16] D. Czarnowski, J. Górski, Sweat ammonia excretion during submaximal cycling exercise, J. Appl. Physiol. 70 (1) (1991) 371–374.

[17] D. Czarnowski, J. Górski, J. Jóźwiuk, A. Boroń-Kaczmarska, Plasma ammonia is the principal source of ammonia in sweat, Eur. J. Appl. Physiol. Occup. Physiol. 65 (2) (1992) 135–137.

[18] D. Czarnowski, J. Langfort, W. Pilis, J. Gorski, Effect of a low-carbohydrate diet on plasma and sweat ammonia concentrations during prolonged nonexhausting exercise, Eur. J. Appl. Physiol. Occup. Physiol. 70 (1) (1995) 70–74.

[19] S.S. Mohiuddin, D. Khattar, Biochemistry, ammonia, StatPearls (2019).

[20] I. Alvear-Ordenes, D. García-López, J. De Paz, J. González-Gallego, Sweat lactate, ammonia, and urea in rugby players, Int. J. Sports Med. 26 (08) (2005) 632–637.

[21] E. Renner, N. Lang, B. Langenstein, M. Struck, T. Bertsch, Validating sweat ammonia as physiological parameter for wearable devices in sports science, in: 2020 42nd Annual International Conference of the IEEE Engineering in Medicine & Biology Society, EMBC, IEEE, 2020, pp. 4644–4647.

[22] B. Martínez-Haya, J.R. Avilés-Moreno, F. Gámez, G. Berden, J. Oomens, Preferential host-guest coordination of nonactin with ammonium and hydroxylammonium, J. Chem. Phys. 149 (22) (2018) 225101.

[23] T. Guinovart, A.J. Bandodkar, J.R. Windmiller, F.J. Andrade, J. Wang, A potentiometric tattoo sensor for monitoring ammonium in sweat, Analyst 138 (22) (2013) 7031–7038.

[24] D.S. Oertel, D.M. Jank, B. Schmitz, D.N. Lang, Monitoring of biomarkers in sweat with printed sensors combined with sport wearables, in: Proceedings of the 2016 ACM International Joint Conference on Pervasive and Ubiquitous Computing: Adjunct, 2016, pp. 893–898.

[25] A.M. Zamarayeva, N.A. Yamamoto, A. Toor, M.E. Payne, C. Woods, V.I. Pister, Y. Khan, J.W. Evans, A.C. Arias, Optimization of printed sensors to monitor sodium, ammonium, and lactate in sweat, APL Mater. 8 (10) (2020) 100905.

[26] S.T. Keene, D. Fogarty, R. Cooke, C.D. Casadevall, A. Salleo, O. Parlak, Wearable organic electrochemical transistor patch for multiplexed sensing of calcium and ammonium ions from human perspiration, Adv. Healthc. Mater. 8 (24) (2019) 1901321.

[27] N. Coppedè, M. Giannetto, M. Villani, V. Lucchini, E. Battista, M. Careri, A. Zappettini, Ion selective textile organic electrochemical transistor for wearable sweat monitoring, Organ. Electron. 78 (2020) 105579.

[28] F. Torricelli, D.Z. Adrahtas, Z. Bao, M. Berggren, F. Biscarini, A. Bonfiglio, C.A. Bortolotti, C.D. Frisbie, E. Macchia, G.G. Malliaras, et al., Electrolyte-gated transistors for enhanced performance bioelectronics, Nat. Rev. Methods Primers 1 (1) (2021) 1–24.

[29] T. Cramer, A. Campana, F. Leonardi, S. Casalini, A. Kyndiah, M. Murgia, F. Biscarini, Water-gated organic field effect transistors–opportunities for biochemical sensing and extracellular signal transduction, J. Mater. Chem. B 1 (31) (2013) 3728–3741.

[30] L. Suo, O. Borodin, T. Gao, M. Olguin, J. Ho, X. Fan, C. Luo, C. Wang, K. Xu, Water-in-salt electrolyte enables high-voltage aqueous lithium-ion chemistries, Science 350 (6263) (2015) 938–943.

[31] S. Wang, A. Lu, C.-J. Zhong, Hydrogen production from water electrolysis: Role of catalysts, Nano Convergence 8 (2021) 1–23.

[32] N. Nakatsuka, K.-A. Yang, J.M. Abendroth, K.M. Cheung, X. Xu, H. Yang, C. Zhao, B. Zhu, Y.S. Rim, Y. Yang, et al., Aptamer–field-effect transistors overcome debye length limitations for small-molecule sensing, Science 362 (6412) (2018) 319–324.

[33] B. Shkodra, Petrelli M., K.-A. Yang, Tagliaferri A., P. Lugli, L. Petti, N. Nakatsuka, Polymeric integration of structure-switching aptamers on transistors for histamine sensing, Faraday Discussions (2023) To be published.

[34] S.H. Kim, K. Hong, W. Xie, K.H. Lee, S. Zhang, T.P. Lodge, C.D. Frisbie, Electrolyte-gated transistors for organic and printed electronics, Adv. Mater. 25 (13) (2013) 1822–1846.

[35] L. Hu, D.S. Hecht, G. Gruner, Carbon nanotube thin films: Fabrication, properties, and applications, Chem. Rev. 110 (10) (2010) 5790–5844.

[36] B. Shkodra, M. Petrelli, M.A. Costa Angeli, D. Garoli, N. Nakatsuka, P. Lugli, L. Petti, Electrolyte-gated carbon nanotube field-effect transistor-based biosensors: Principles and applications, Appl. Phys. Rev. 8 (4) (2021) 041325.

[37] S. Hamed, P. Ibba, M. Petrelli, M. Ciocca, P. Lugli, L. Petti, Transistor-based plant sensors for agriculture 4.0 measurements, in: 2021 IEEE International Workshop on Metrology for Agriculture and Forestry, MetroAgriFor, IEEE, 2021, pp. 69–74.

[38] G. Elli, S. Hamed, M. Petrelli, P. Ibba, M. Ciocca, P. Lugli, L. Petti, Field-effect transistor-based biosensors for environmental and agricultural monitoring, Sensors 22 (11) (2022) 4178.

[39] A. Molazemhosseini, F.A. Viola, F.J. Berger, N.F. Zorn, J. Zaumseil, M. Caironi, A rapidly stabilizing water-gated field-effect transistor based on printed single-walled carbon nanotubes for biosensing applications, ACS Appl. Electron. Mater. 3 (7) (2021) 3106–3113.

[40] S. Joshi, V.D. Bhatt, E. Jaworska, M. Becherer, K. Maksymiuk, A. Michalska, P. Lugli, Using lipophilic membrane for enhanced-performance aqueous gated carbon nanotube field effect transistors, Physica Status Solidi (A) 215 (11) (2018) 1700993.

[41] B. Shkodra, M. Petrelli, M.A. Costa Angeli, A.S. Inam, E. Avancini, N. Münzenrieder, P. Lugli, L. Petti, Flexible carbon nanotube-based electrolyte-gated field-effect transistor for spermidine detection, in: 2021 IEEE International Conference on Flexible and Printable Sensors and Systems, FLEPS, IEEE, 2021, pp. 1–4.

[42] A. Falco, L. Cinà, G. Scarpa, P. Lugli, A. Abdellah, Fully-sprayed and flexible organic photodiodes with transparent carbon nanotube electrodes, ACS Appl. Mater. Interfaces 6 (13) (2014) 10593–10601.

[43] F. Loghin, A. Rivadeneyra, M. Becherer, P. Lugli, M. Bobinger, A facile and efficient protocol for preparing residual-free single-walled carbon nanotube films for stable sensing applications, Nanomaterials 9 (3) (2019) 471.

[44] M. Petrelli, B. Shkodra, M.A. Costa Angeli, A. Scarton, S. Pogliaghi, R. Biasi, P. Lugli, L. Petti, Flexible, planar, and stable electrolyte-gated carbon nanotube field-effect transistor-based sensor for ammonium detection in sweat, in: 2022 IEEE International Flexible Electronics Technology Conference, IFETC, IEEE, 2022, pp. 1–2.

[45] M. Petrelli, B. Shkodra, M.A. Costa Angeli, A. Scarton, S. Pogliaghi, R. Biasi, P. Lugli, L. Petti, Novel gate electrode design for flexible planar electrolyte-gated field-effect transistor-based sensors for real-time ammonium detection, in: 2022 IEEE Sensors, IEEE, 2022, pp. 1–4.

[46] B. Shkodra, M. Petrelli, M.A. Costa Angeli, A.S. Inam, P. Lugli, L. Petti, Optimization of the spray-deposited carbon nanotube semiconducting channel for electrolyte-gated field-effect transistor-based biosensing applications, IEEE Sens. J. (2022).

[47] A. Michalska, K. Pyrzyńska, K. Maksymiuk, Method of achieving desired potentiometric responses of polyacrylate-based ion-selective membranes, Anal. Chem. 80 (10) (2008) 3921–3924.

[48] K.B. Oldham, A Gouy–Chapman–Stern model of the double layer at a (metal)/(ionic liquid) interface, J. Electroanal. Soc. 613 (2) (2008) 131–138.
[49] T. Sokalski, A. Ceresa, M. Fibbioli, T. Zwickl, E. Bakker, E. Pretsch, Lowering the detection limit of solvent polymeric ion-selective membrane electrodes. 2. influence of composition of sample and internal electrolyte solution, Anal. Chem. 71 (6) (1999) 1210–1214.
[50] J. Waswa, J. Irudayaraj, C. DebRoy, Direct detection of e. coli o157: H7 in in selected food systems by a surface plasmon resonance biosensor, LWT-Food Sci. Technol. 40 (2) (2007) 187–192.
[51] M.R. Islam, A. Iftekher, K.R. Hasan, M. Nayen, S.B. Islam, R. Islam, R.L. Khan, E. Moazzam, Z. Tasnim, et al., Surface plasmon resonance based highly sensitive gold coated PCF biosensor, Appl. Phys. A 127 (2) (2021) 1–12.
[52] M. Petrelli, A. Golparvar, A. Meimandi, B. Shkodra, M.A.C. Angeli, A. Falco, P. Lugli, L. Petti, S. Carrara, Flexible sensor and readout circuitry for continuous ion sensing in sweat, IEEE Sensors Lett. 7 (6) (2023).